

# The Addition of Baldwin-Lomax Turbulence Model to LeMANS

Abhilasha Anna

August 30, 2010

## List of Symbols

$A^+$	damping factor
$D$	diffusivity
$F_{MAX}$	maximum of function $F(y)$ Eq.(16)
$F_{KLEB}$	Klebanoff intermittency factor
$k$	thermal conductivity
$l$	mixing length
$M_\infty$	Mach number
$P_w$	pressure at the wall
$Pr$	Prandtl number
$Pr_t$	turbulent Prandtl number
$Q_w$	heat flux at the wall
$T_\infty$	free stream temperature
$T_w$	wall temperature
$T_{aw,ideal}$	ideal adiabatic wall temperature $T_\infty(1 + \frac{1}{2}(\gamma - 1)M_\infty^2)$
$u, v, w$	Velocity components in the x,y,z directions
$u^+$	mean velocity normalized by friction velocity $u/u_\tau$
$u_\tau$	friction velocity $\sqrt{\tau_w/\rho_w}$
$U_\infty$	free stream velocity
$y$	normal distance from the wall
$y_{crossover}$	smallest value of $y$ at which the values from $\mu_{t,inner}$ and $\mu_{t,outer}$ Eq.(9) are equal
$y^+$	law of the wall coordinate $\rho_w u_\tau y / \mu_w$
$y_{MAX}$	value of $y$ at which function $F(y)$ Eq.(16) is maximum
$\delta$	boundary layer thickness
$\omega$	vorticity
$\mu_w$	viscosity at the wall
$\mu_t$	eddy viscosity
$\mu_\infty$	free stream eddy viscosity
$\mu_{t,inner}$	eddy viscosity from inner law
$\mu_{t,outer}$	eddy viscosity from outer law
$\nu_t$	kinematic eddy viscosity
$\rho_w$	density at the wall
$\rho_\infty$	free stream density
$\tau_w$	shear stress at the wall
$\tau$	local shear stress

# 1 Introduction

The Baldwin-Lomax eddy viscosity model [1] has been added to the existing flow field solver LeMANS [10]. In this work turbulent flow over a flat plate has been modeled. Results for the shear stress and heat transfer predictions along the plate and their comparison with the experimental data as well other numerical calculations are presented. The model provides good agreement with the experimental data and other numerical results. The work involves the study using the original and a modified Baldwin-Lomax Model. The effect of the different wall conditions viz. hot and cold has been studied using the two models. A brief discussion on the theory behind algebraic turbulence models has been provided, followed by the original Baldwin-Lomax model and the modification made to the turbulence model. The modifications employed in the implementation of the model to LeMANS have been presented, followed by the discussion of the results and conclusions from the study.

## 1.1 Structure of a Turbulent Boundary Layer

A turbulent boundary layer profile is composed of an inner and outer layer and an intermediate overlap layer between the two. In the inner layer, the response of the fluid is dominated by the viscous (molecular) shear and in the outer layer, turbulent (eddy) shear dominates. In the overlap layer, both types of shear are important. The inner layer is much smaller than the outer layer. In the inner layer, the mean velocity profile would depend upon the wall shear stress  $\tau_w$ , fluid properties and distance  $y$  from the wall and independent of free stream parameters. The expression obtained is known as the *law of the wall*, given by:

$$u^+ = f(y^+) \quad (1)$$

The inner layer is composed of three layers viz. viscous sublayer, buffer layer and fully turbulent layer i.e. the log layer. In the viscous sublayer, there is a linear relation between  $u^+$  and  $y^+$ . The viscous stresses dominate since the turbulent fluctuations become zero at the wall. The buffer layer is the region where the flow is partly viscous and partly turbulent. The log layer is the region where viscosity has little effect and the flow is fully turbulent.

The outer layer is independent of viscosity but dependent on the wall shear stress  $\tau_w$ , boundary layer thickness and freestream pressure gradient. The wall acts a source of retardation of the freestream velocity and thus the outer layer is defined by the *velocity defect law*, given by:

$$\frac{U_\infty - u}{u_\tau} = f\left(\frac{y}{\delta}\right) \quad (2)$$

The different layers [8] have been defined on the basis of  $y^+$ . The various layers and their corresponding  $y^+$  that are used to describe near-wall flow are given in Table 1.

Table 1: *Wall layers*

Layer	Location ( $y^+$ )
Viscous sublayer	$y^+ < 5$
Buffer layer	$5 < y^+ < 30$
Log layer	$y^+ > 30$
Outer layer	$y^+ > 50$

The law of the wall for compressible flow is deduced from the law for incompressible flow. The formula is called *Van Driest Transformation*. It can be regarded as transforming the inner-layer part of the compressible boundary layer profile to an equivalent incompressible flow  $u_{eq}$  that obeys the logarithmic formula. It is given by the following relation [11] :

$$u_{eq} = \frac{U_\infty}{a} \left( \sin^{-1} \frac{2a^2 u / U_\infty - b}{Q} + \sin^{-1} \frac{b}{Q} \right) \quad (3)$$

$$\text{where } a = \left( \frac{\gamma - 1}{2} M_\infty^2 \frac{T_\infty}{T_w} \right)^{1/2} \quad b = \left( \frac{T_{aw}}{T_w} - 1 \right) \quad Q = (b^2 + 4a^2)$$

## 1.2 Algebraic Turbulence Model

An accurate calculation of velocity and temperature boundary layer profiles in turbulent flows is limited because of the presence of fluctuation terms in the governing equations (Navier-Stokes equations)[3]. At present, there is no relation that correctly relates the fluctuation terms to the dependent variables. The Direct Numerical Simulation (DNS) of the instantaneous Navier-Stokes equations for turbulent flows can give promising results but the computer requirements for such an approach are large. Several models have been proposed for the Reynolds stress i.e. the fluctuation term. Algebraic turbulence models based on Prandtl's mixing length theory and eddy viscosity concept are examples of such models. They relate the Reynolds stress to the local mean velocity gradient. The implementation of such models is less complicated as compared to the one equation or two equation models and require less computational time.

Boussinesq gave the concept of eddy viscosity to model the Reynolds shear stress by assuming that turbulent stress acts like the viscosity stresses. This implies that the turbulent stresses are proportional to the velocity gradient. This is defined by the following equation:

$$-\overline{\rho u'_i u'_j} = \rho \nu_t \left( \frac{\partial u_i}{\partial x_j} + \frac{\partial u_j}{\partial x_i} \right) \quad (4)$$

where  $\nu_t$  is the eddy kinematic viscosity and is approximated as the product of velocity and length scale i.e.

$$\nu_t = \text{length} \times \text{velocity}$$

According to the mixing length concept proposed by Prandtl, the Reynolds shear stress is calculated from,

$$-\overline{\rho u'_i u'_j} = \rho l^2 \left( \frac{\partial u_i}{\partial x_j} + \frac{\partial u_j}{\partial x_i} \right) \left( \frac{\partial u_i}{\partial x_j} + \frac{\partial u_j}{\partial x_i} \right) \quad (5)$$

where  $l$  is the characteristic turbulence length scale and needs to be defined. Comparing (4) and (5), the relationship between eddy viscosity and mixing length is given by:

$$\nu_t = l^2 \left( \frac{\partial u_i}{\partial x_j} + \frac{\partial u_j}{\partial x_i} \right) \quad (6)$$

Experimental data is used to define  $l$  and  $\nu_t$ . The distribution of  $l$  across a boundary layer is given by two empirical functions that define the fully turbulent part of the inner layer and the outer layer.

Therefore,

$$\begin{aligned} l_i &= Ky & y_o \leq y \leq y_c \\ l_o &= \alpha_1 y & y_c \leq y \leq \delta \end{aligned} \quad (7)$$

where  $y_o$  is a small distance from the wall and  $y_c$  is obtained from the continuity of  $l$ .  $l_i$  and  $l_o$  are the mixing length for the inner and outer layer respectively. From experimental data, the value of  $K$  and  $\alpha_1$  are taken to be 0.40 and 0.75 respectively.

The mixing length expression apply in the fully turbulent part of the boundary layer except for the sublayer and buffer layer close to the wall. Van Driest [5] proposed a modification to account for these layers defining the mixing length as

$$L = l [1 - \exp(-y/A)] \quad (8)$$

where  $A=26$ .

Several algebraic eddy viscosity models have been developed based on the above concept. Examples are Baldwin-Lomax (BL), Cebeci-Smith (CS), Mellor-Herring (MR) model. The boundary layer is composed of the inner and outer layer in all these models. Out of these models, Baldwin-Lomax model has been implemented in LeMANS and tested for boundary layer flow and is discussed in detail in the following section.

### 1.2.1 Baldwin-Lomax Model

This model is based on the CS [2] model with modifications in the expressions for eddy viscosity that dont require the need to determine the the edge of the boundary layer. The basic governing equations are the Navier-Stokes equations. The effects of turbulence are incorporated by replacing the molecular coefficient of viscosity  $\mu$  with  $\mu + \mu_t$  in the stress term and replacing  $k/C_p = \mu/Pr$  with  $\mu/Pr + \mu/Pr_t$  in the heat flux term. The eddy viscosity  $\mu_t$  is given by:

$$\mu_t = \begin{cases} (\mu_t)_{inner}, & y \leq y_{crossover} \\ (\mu_t)_{outer}, & y_{crossover} \leq y \end{cases} \quad (9)$$

The Prandtl-Van Driest formulation is used in the inner region given by:

$$(\mu_t)_{inner} = \rho l^2 |\omega| \quad (10)$$

where,

$$l = Ky [1 - \exp(-y^+/A^+)] \quad (11)$$

$|\omega|$  is the magnitude of vorticity given by

$$|\omega| = \sqrt{\left(\frac{\partial u}{\partial y} - \frac{\partial v}{\partial x}\right)^2 + \left(\frac{\partial v}{\partial z} - \frac{\partial w}{\partial y}\right)^2 + \left(\frac{\partial w}{\partial x} - \frac{\partial u}{\partial z}\right)^2} \quad (12)$$

and

$$y^+ = \frac{\rho_w u_{\tau} y}{\mu_w} \quad (13)$$

The following formulation is used to define the eddy viscosity in the outer region,

$$(\mu_t)_{outer} = KC_{CP}\rho F_{WAKE}F_{KLEB}(y) \quad (14)$$

where  $K$  is the Clauser constant,  $C_{CP}$  is an additional constant, and

$$F_{WAKE} = \begin{cases} y_{MAX}F_{MAX} \\ or \\ C_{WK}y_{MAX}u_{DIF}^2/F_{MAX} \end{cases} \quad (15)$$

The quantities  $y_{MAX}$  and  $F_{MAX}$  are determined from the vorticity function:

$$F(y) = y |\omega| [1 - \exp(-y^+/A^+)] \quad (16)$$

In wakes, the exponential term is set equal to zero. For the case of boundary layers,  $F_{WAKE} = y_{MAX}F_{MAX}$  has been used. The quantity  $F_{MAX}$  is the maximum value of  $F(y)$  that occurs in a profile at a fixed  $x$  station and  $y_{MAX}$  is the value of  $y$  at which it occurs. Therefore, the maximum in the vorticity function is used to define the length scale for the outer layer. The quantity  $u_{DIFF}$  is the difference between maximum and minimum total velocity in the profile.

The Baldwin-Lomax model cannot predict the transition point although it can be specified as a user input. The transition to turbulence can be predicted by setting  $\mu_t$  equal to zero everywhere in a profile for which the maximum value of  $\mu_t$  calculated from the above relations is less than a specified value. It is given by,

$$\mu_t = 0 \quad \text{if } \mu_{t,\max \text{ in profile}} < C_{MUTM}\mu_{inf} \quad (17)$$

For purpose of study, the turbulence model is enabled from the leading edge i.e.  $C_{MUTM}$  is set to zero.

The constants that appear in the above relations are as follows:

$$\begin{aligned}
A^+ &= 26.0 \\
C_{CP} &= 1.6 \\
C_{KLEB} &= 0.3 \\
C_{WK} &= 0.25 \\
C_{MUTM} &= 14.0 \\
k &= 0.4 \\
K &= 0.0168 \\
Pr &= 0.72 \\
Pr_t &= 0.9
\end{aligned}$$

Two modifications to the original BL model have been made to account for the flows with pressure gradients. First, the local values for density  $\rho$  and eddy viscosity  $\mu$  are used instead of the wall values to find  $y^+$  i.e.

$$y^+ = \frac{\rho u \tau y}{\mu} \quad (18)$$

Therefore, the equations (13) and (19) differ by the factor:

$$Y = \sqrt{\frac{\rho}{\rho_w} \frac{\mu_w}{\mu}} \quad (19)$$

This factor plays a significant role in the case of cold wall boundary layers. This is shown and discussed in the results section in detail.

Second,  $A^+$  has been modified, given by

$$A^+ = 26 \left( \frac{|\tau|}{\tau_w} \right)^{-1/2} \quad (20)$$

where  $\tau$  is the local shear stress. This modified definition of  $A^+$  is suggested by [6] and thus the model is referred to as modified Baldwin Lomax Model.

## 2 Implementation of Baldwin-Lomax to LeMANS

The following gives a description of what changes have been made to the root version of LeMANS to incorporate the BL turbulence model. Three sub routines viz. `find_wall.c`, `calc_new_viscosity.c` and `lomax.c` have been added.

The BL model is based on calculating the values in each profile i.e. at a fixed  $x$  station. For example, the quantity  $F_{MAX}$  is the maximum value of  $F(y)$  that occurs in a profile at a fixed  $x$  station and  $y_{MAX}$  is the value of  $y$  at which it occurs. Therefore, nearest wall corresponding to each cell to be identified that serves as a  $x$  station. The values of  $F_{MAX}$  for each profile is stored at the corresponding nearest wall after finding the maximum of  $F(y)$  for each cell corresponding to a common wall. The nearest wall is calculated in `find_wall.c`.

The values  $\tau_w, \rho_w, \mu_w, |\tau|$  and  $|\omega|$  are calculated in `calc_viscous_residue.c`. The turbulent eddy viscosity using the BL model is calculated in `calc_new_viscosity.c`. It calls `lomax.c` to calculate  $(\mu_t)_{inner}$  and  $(\mu_t)_{outer}$ . The values of the three transport coefficients i.e.  $\mu, k$  and  $D$  are updated in the end. `calc_new_viscosity` is called by `update.c` to update the values of the transport coefficients.

A quadratic curve fit is used for the determination of  $F_{MAX}$  and  $y_{MAX}$  from the function  $F(y)$ . Since the solution is discretized, position and value of the maximum  $F_{MAX}$  and hence the  $y_{MAX}$  could be incorrect. This could result in a jump in the value of  $\mu_t$  from one profile to another as can be seen in Fig.1 The discrete values in the vicinity of  $F_{MAX}$  are taken and are fitted by a quadratic fit. The curve fit results in a smoother variation of  $F_{MAX}$  and  $y_{MAX}$  from one profile to another. This could be seen in Fig. 3.  $y_{MAX}$  denotes the discretized value of  $y_{MAX}$  and  $y_{MAXfit}$  denotes the  $y_{MAX}$  after curve fit. As can be seen in Fig.2, the  $\mu_t$  contour is smoother as opposed to the one shown in Fig.1. Another curve fit method i.e. the over-lapping parabola technique was used to find the maximum but the results obtained were not good.

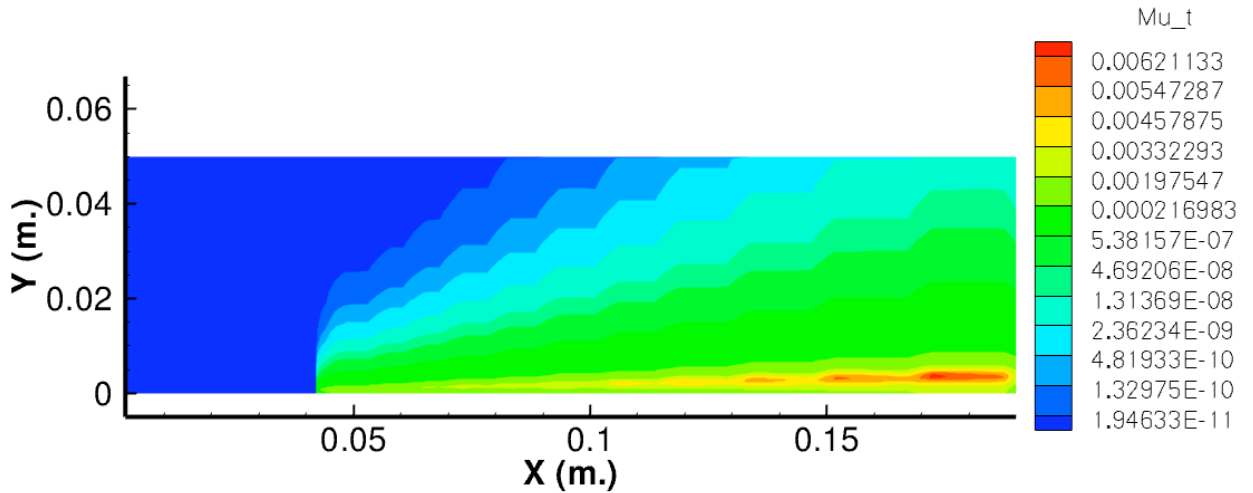


Figure 1: Profile of  $\mu_t$  without the curve fit



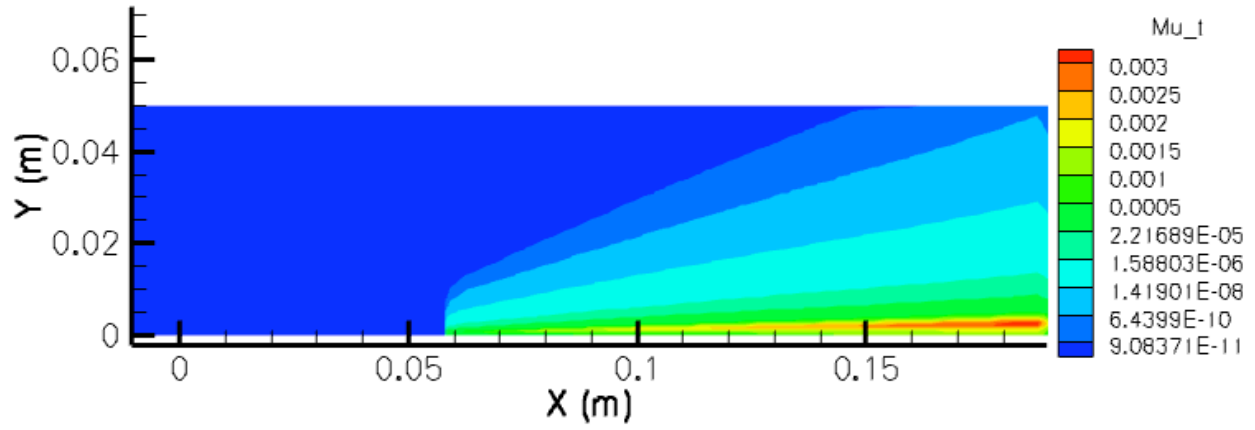


Figure 2: Profile of  $\mu_t$  with the curve fit

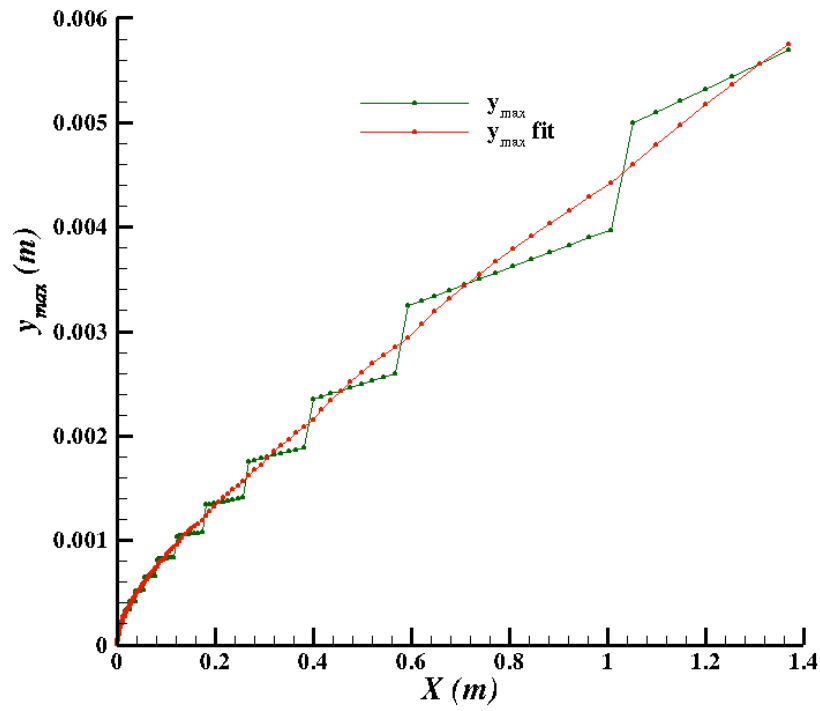


Figure 3: Plot of  $y_{max}$  Vs.  $X$  showing the discretized and curve-fit value of  $y_{max}$

### 3 Results

#### 3.1 Grids Used

A grid study for the  $M = 11$  cold wall case was conducted using the Baldwin-Lomax model on a fine grid, along with two successive grids referred to as medium and coarse grids. Their specification is given in Table 2.

Table 2: *Grids used and their size*

Grid Reference Name	$N_x$	$N_y$	$\delta y_{\text{leading edge}}$
Coarse	130	50	4e-6
Medium	250	50	2e-6
Fine	250	100	1e-6

The fine grid employed was  $250 \times 100$ , with 220 points on the plate and 30 points leading up to the plate. The medium grid employed was  $250 \times 50$ , with 220 points on the plate and 30 points leading up to the plate. The coarse grid employed was  $130 \times 50$ , with 110 points on the plate and 20 points leading up to the plate. There was a streamwise clustering near the plate leading edge, as shown in Figure 4. Results for the shear stress and heat transfer obtained using the three grids used are plotted in Figure 5 and Figure 6 respectively. It can be seen that all three grids yielded very close results away from the plate leading edge. The biggest differences were at the plate leading edge. The results for the medium grid as compared to the coarse grid were closer to the fine grid over most of the plate. The medium has been used to obtain all the results.

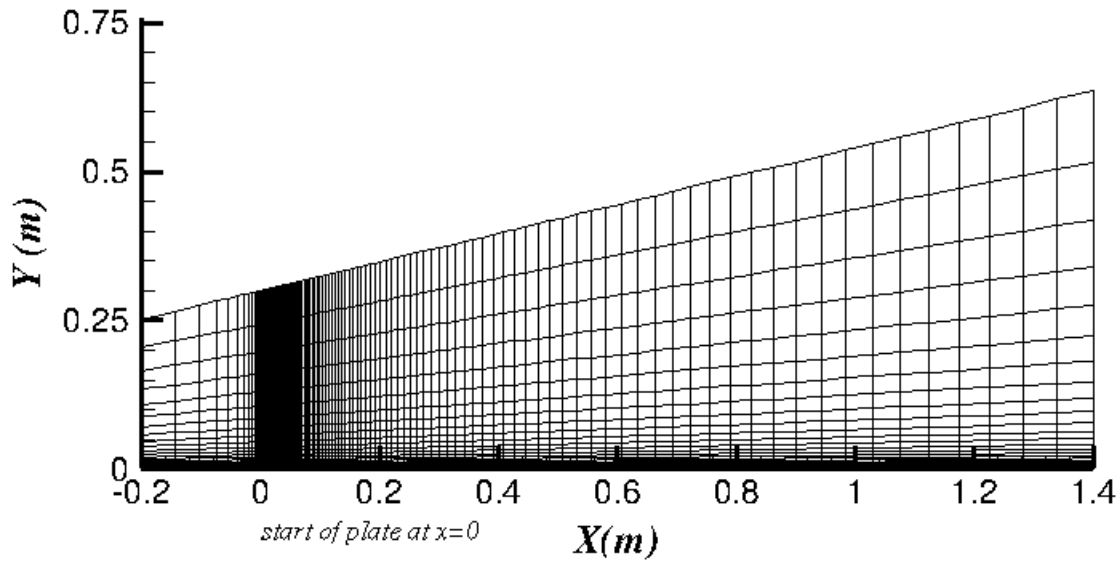


Figure 4: *Flat plate grid*

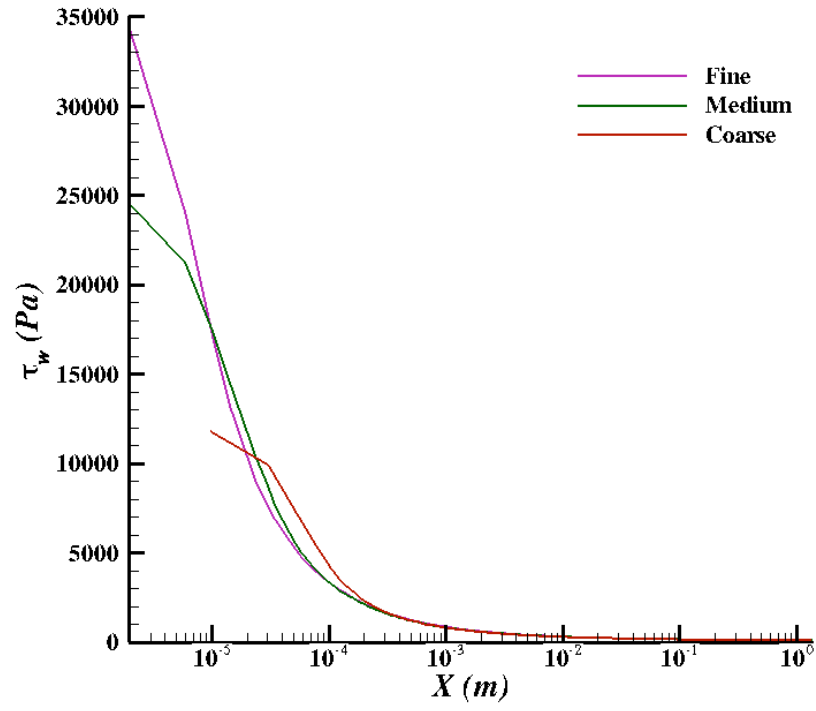


Figure 5: *Shear stress grid study on three successive grid sizes*

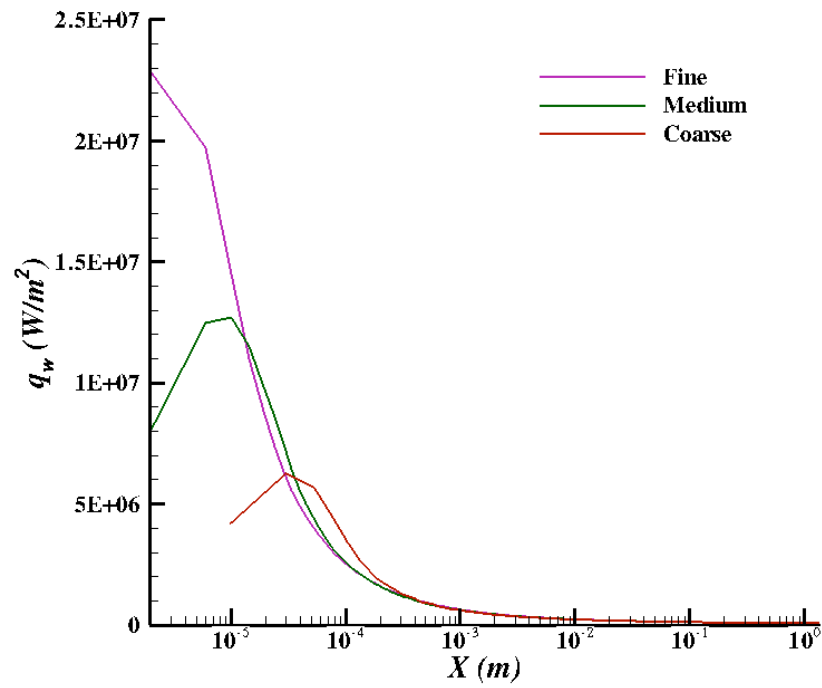


Figure 6: *Heat transfer grid study on three successive grid sizes*

### 3.2 Verification and Results

The hypersonic turbulent flow over a flat plate has been tested for different kinds of wall conditions viz. hot wall, cold wall and adiabatic wall. It is a case of cold wall if there is a heat transfer from the flow to the wall i.e.  $T_w < T_{aw}$ . The opposite case would be that of a hot wall where the heat is transferred from the wall into the flow i.e.  $T_w > T_{aw}$ .

For the purpose of this study, a Mach 11 flow of air over a 52 inch flat plate at zero angle of attack investigated experimentally by Holden [7] is used as a test case to assess the accuracy of the Baldwin-Lomax turbulence model. The results are compared to the experimental data and simulation results from the NASA Langley's code LAURA. The results for hot wall and adiabatic wall have been provided using the same test conditions with a different wall temperature. All the results are obtained using the local values unless otherwise mentioned. In all the cases, the turbulence model is enabled from the leading edge. Although, there is an option of setting the transition location in the code by specifying the value of  $C_{MUTM}$ .

Flow conditions for Mach 11 Cold Wall flat plate case are given as:

$$\begin{aligned} M &= 11.1 \\ U_\infty &= 1780 \text{ m/s} \\ T_\infty &= 64 \text{ K} \\ T_w &= 296.66 \text{ K} \\ T_{aw,ideal} &= 1641.08 \text{ K} \\ T_w/T_{aw,ideal} &= 0.18 \\ \rho_\infty &= 0.09483 \text{ kg/m}^3 \end{aligned}$$

The results for the turbulent flow using the cold wall conditions are plotted in Figure 7 , Figure 8 and Figure 9 for shear stress, heat transfer and pressure at the wall respectively. It can be seen that the results are in excellent agreement with results from Langley LAURA. The results are in reasonable agreement with the experimental data. The experimental data is provided for shear stress and heat transfer.

The Mach 11 cold wall test case is also used for predicting hypersonic laminar flow over a flat plate. The results for the laminar flow using the cold wall conditions are plotted in Figure 10 , Figure 11 and Figure 12 for shear stress, heat transfer and pressure at the wall respectively and are compared with Langley LAURA computational results. The results show an excellent agreement with the simulation results.

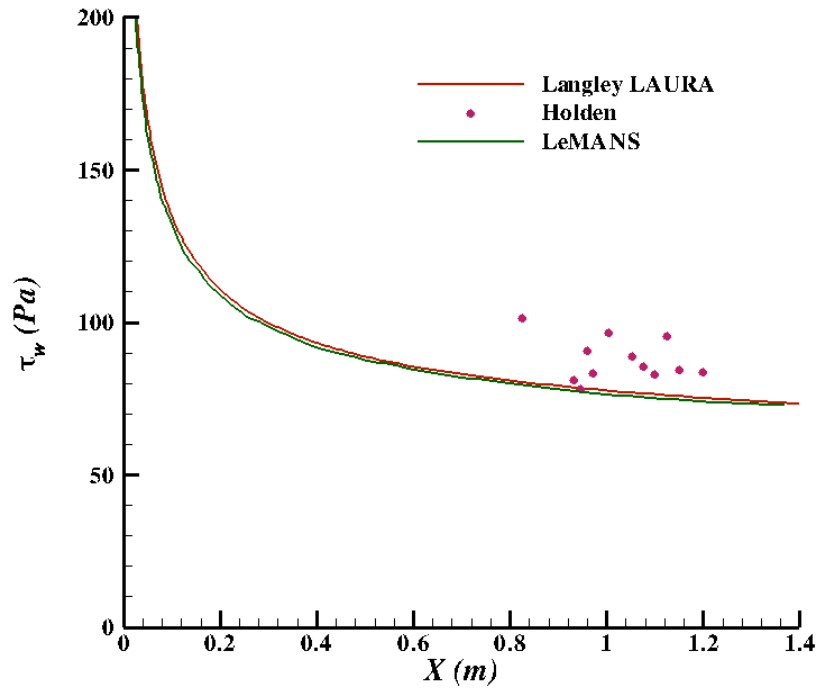


Figure 7:  $\tau_w$  Vs  $X$

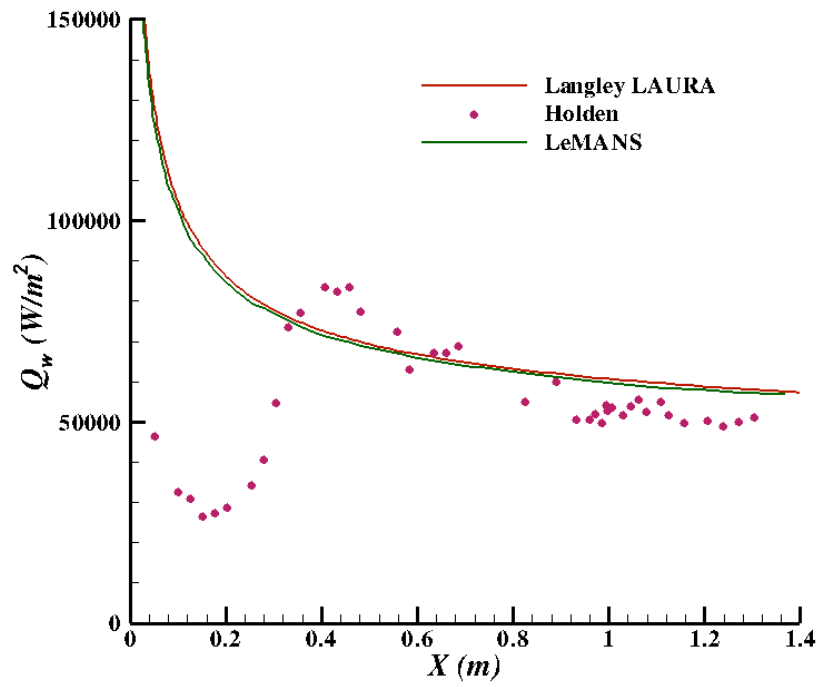


Figure 8:  $Q_w$  Vs  $X$

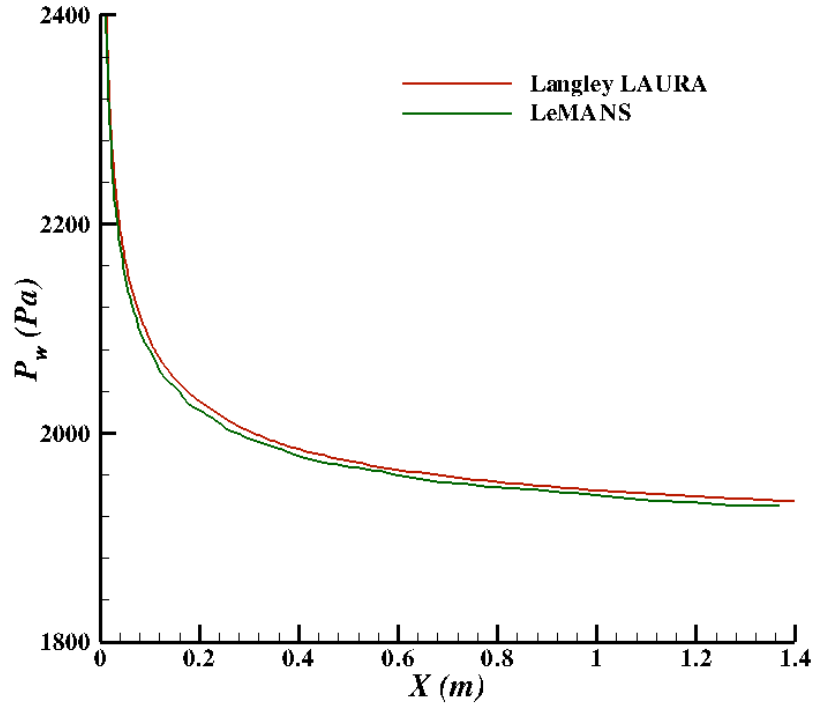


Figure 9:  $P_w$  Vs  $X$

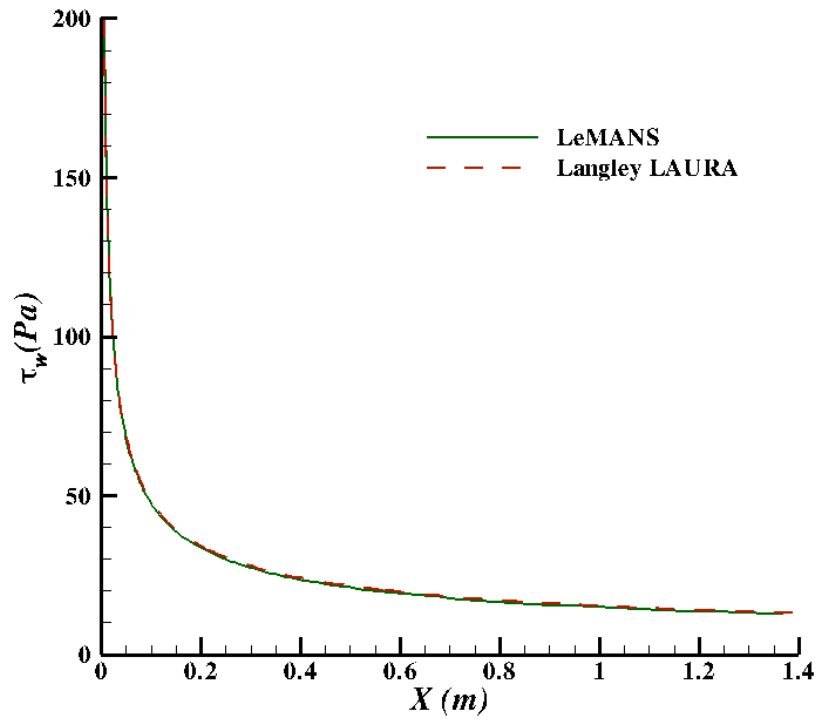


Figure 10:  $\tau_w$  Vs  $X$

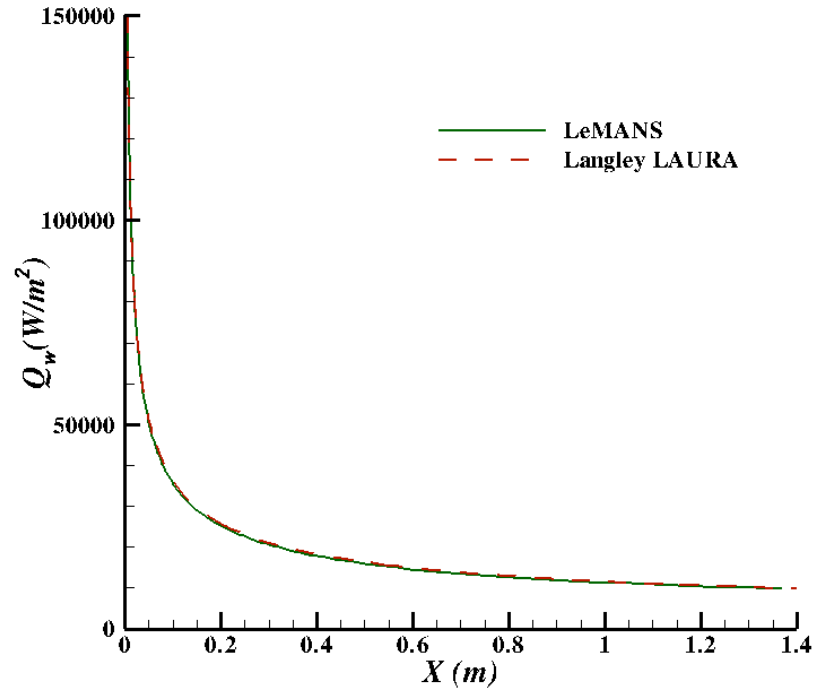


Figure 11:  $Q_w$  Vs  $X$

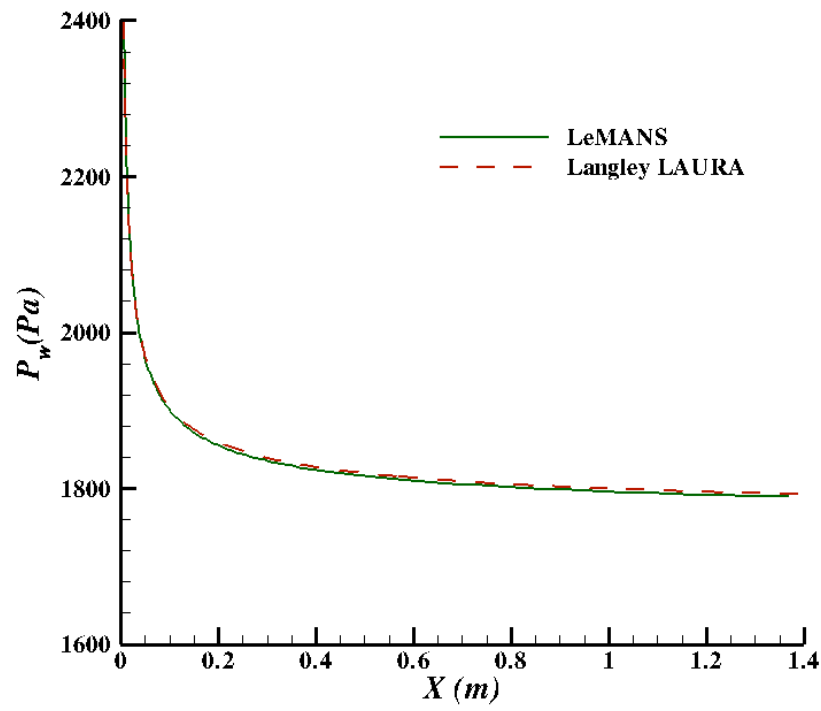


Figure 12:  $P_w$  Vs  $X$

Flow conditions for Mach 11 Hot and Adiabatic wall flat plate case:

$$M=11.1$$

$$U_{inf} = 1780 \text{ m/s}$$

$$T_{inf} = 64 \text{ K}$$

$$T_w = 1641.08 \text{ K (For Adiabatic Wall)}$$

$$T_w/T_{aw,ideal} = 1.0 \text{ (For Adiabatic Wall)}$$

$$T_w = 2560 \text{ K (For Hot Wall)}$$

$$T_w/T_{aw,ideal} = 1.55 \text{ (For Hot Wall)}$$

$$\rho_{inf} = 0.09483 \text{ kg/m}^3$$

Figure 13 and Figure 14 show the comparison of the results for the shear stress when local and wall values are used to find the eddy viscosity with cold and hot wall condition respectively. Figure 15 and Figure 16 shows the comparison of the results for the heat transfer. These two cases show the effect of wall temperature on the results. It clearly shows that the shear stress is over predicted when the wall values are used in the case of a cold wall case. It is said that the Baldwin-Lomax model performs better with local values especially in case of a cold wall [4, 9]. For hot walls, the two values give slightly different results but for cold walls the results differ significantly. Also the wall values are below the local values for the hot wall case. The wall value predictions for shear stress are 20% above the local value results for the cold wall case and 12 % below the local value results for the hot wall case. The wall values predictions for heat transfer are 20% above the local value results for the cold wall case and 6 % below the local value results for the hot wall case. The results of the original BL model are referred to as wall values results and the results for modified BL model are referred to as local values results.



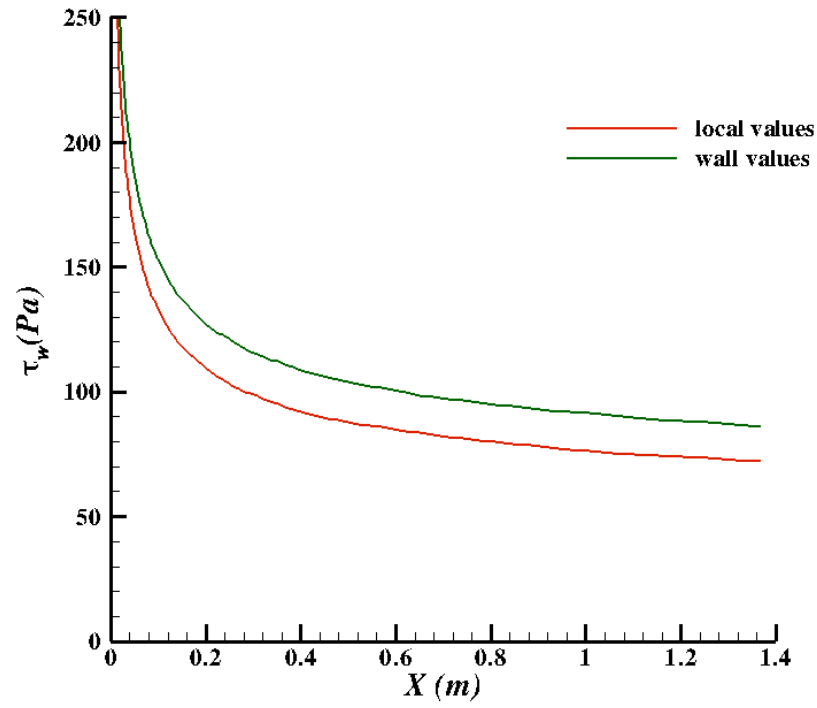


Figure 13:  $\tau_w$  Vs  $X$  for Cold Wall Case

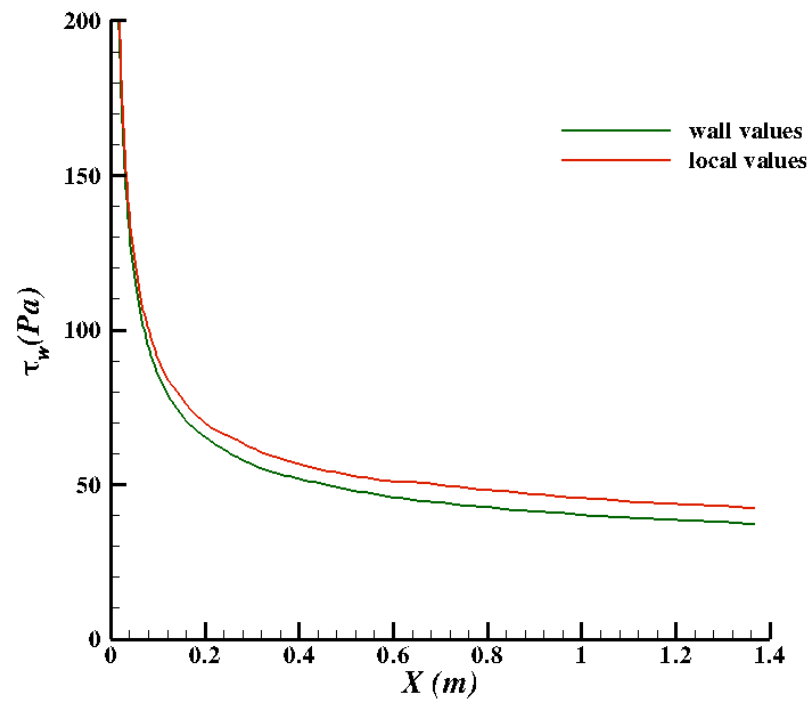


Figure 14:  $\tau_w$  Vs  $X$  for Hot Wall Case

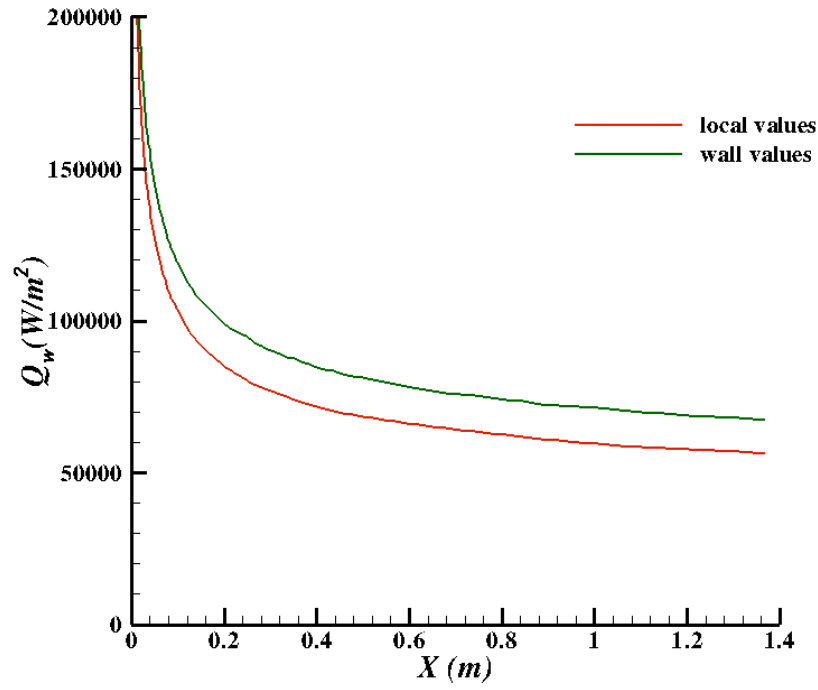


Figure 15:  $Q_w$  Vs  $X$  for Cold Wall Case

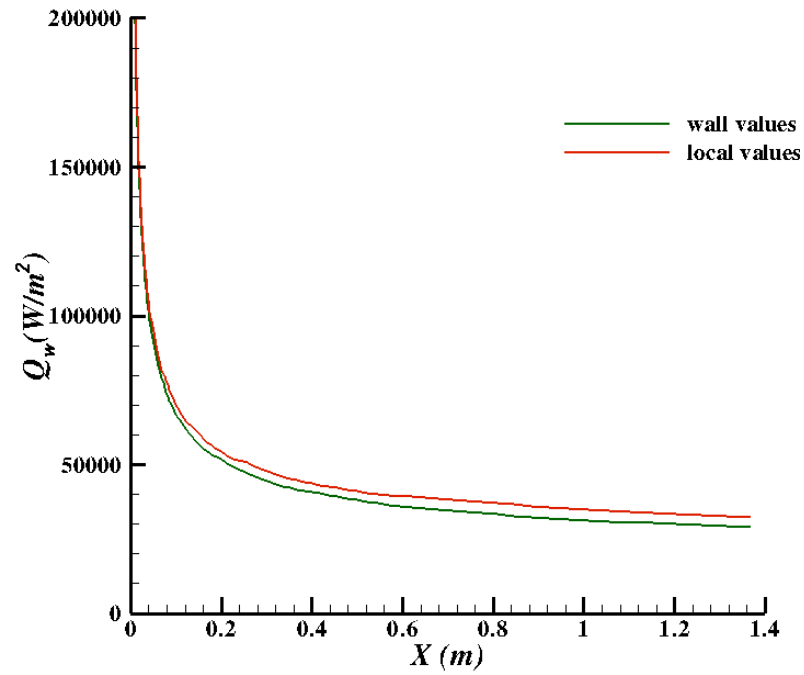


Figure 16:  $Q_w$  Vs  $X$  for Hot Wall Case

Figure 17 shows the comparison of the results for the shear stress when local and wall values are used to find the eddy viscosity with adiabatic wall condition. The trend of the results is similar to the one obtained from the hot wall condition. The wall value predictions for shear stress are 7.67 % below the local value results for the adiabatic wall case.

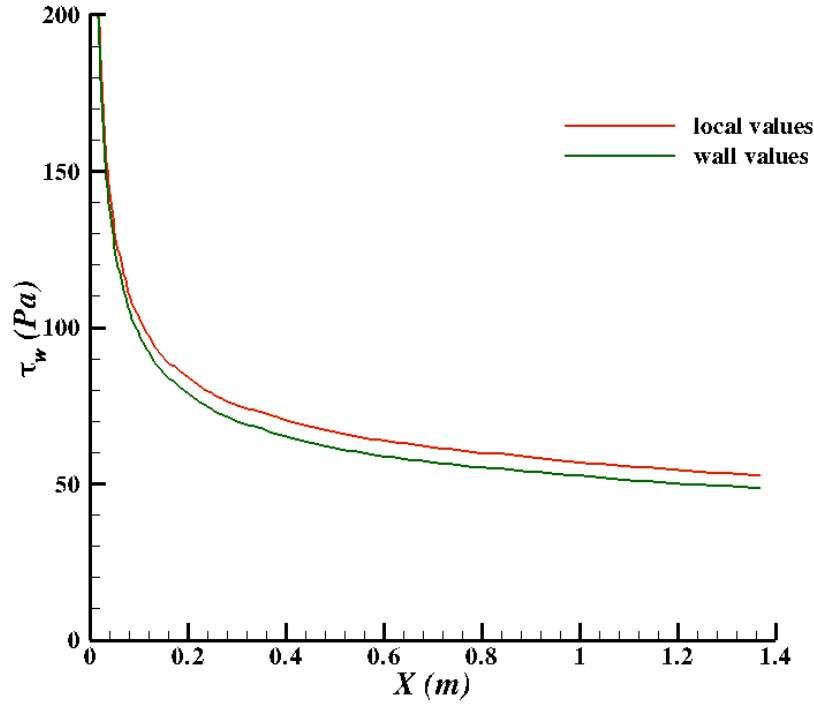


Figure 17:  $\tau_w$  Vs  $X$  for Adiabatic Wall Case

Figure 18 shows the result for the Mach 11 flat plate case showing the comparison using different definition of  $A^+$  in the determination of length scale. It shows that  $A^+$  can be taken as a constant in the case of a flat plate as there is no difference in the results. The local values play a significant role in the case of a flat plate. The eddy viscosity is largely affected by the local values that define the friction velocity.

A plot of non-dimensional eddy viscosity in the inner and outer layer both for the local as well as the wall values at  $x = 1\text{m}$ . is shown in Figure 19. The eddy viscosity is larger for the formulation using wall values as compared the one using local values. The peak wall value eddy viscosity is 31 % higher than the peak local value eddy viscosity.

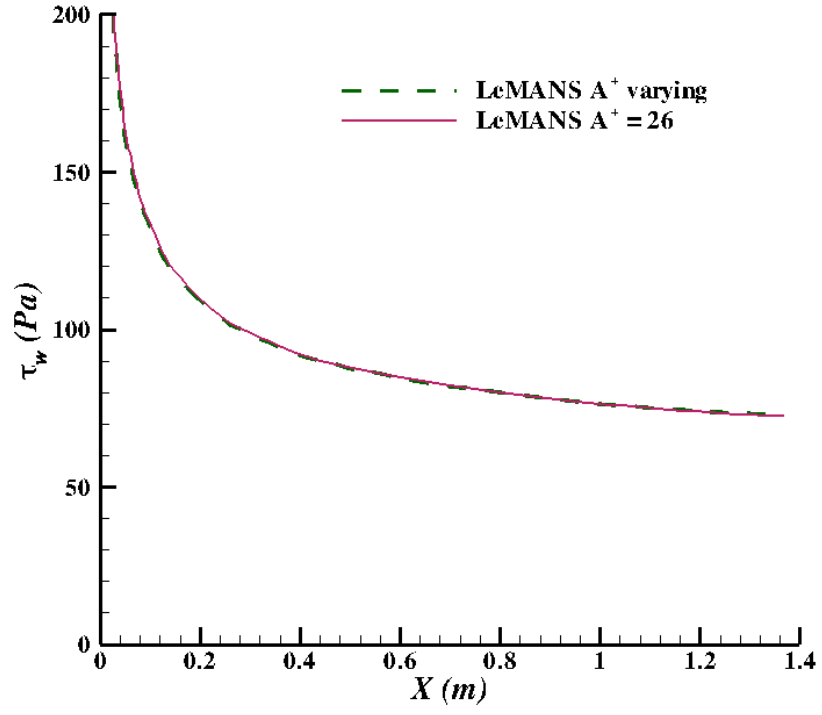


Figure 18:  $\tau_w$  Vs  $X$

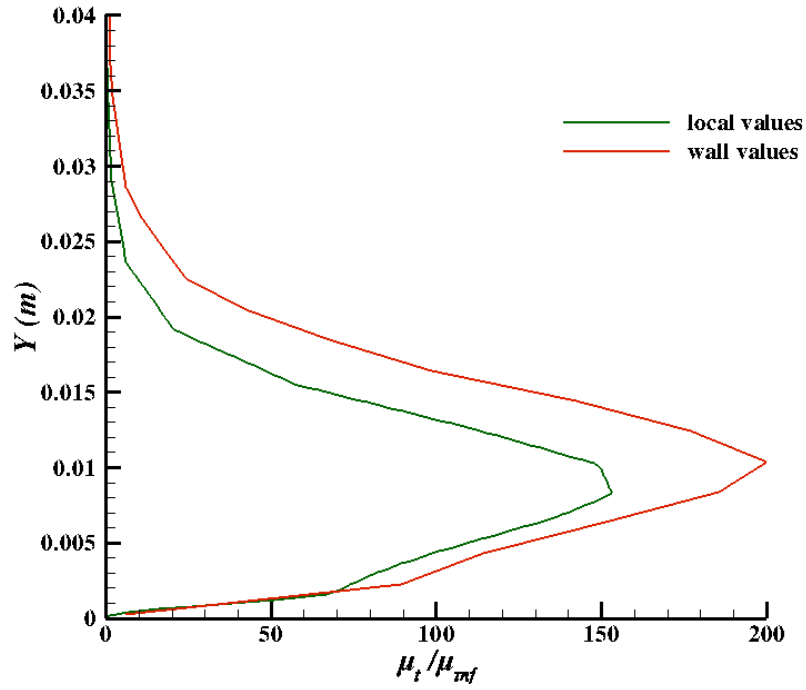


Figure 19: *Turbulent eddy viscosity profile at  $x=1$  m.*

### 3.3 Comparison with Van Driest Transformation

Van Driest transformation given by Eq. 3 is used to analytically compare the turbulent boundary layer profile. Based on the computed values of velocity profile, the transformed profile is plotted in Figure 20 along with the computed profile. There is good agreement with the transformed profile in the inner layer. The transformation given by Eq. 3 is primarily defined for the inner layer. Applying the transformation in the outer layer results in profile qualitatively close to the computed profile. The  $U^+$  profile is affected by the value of  $y^+$ . It is shown in Figure 21 where  $U^+$  Vs.  $y^+$  is plotted for two different values of  $y^+$ .

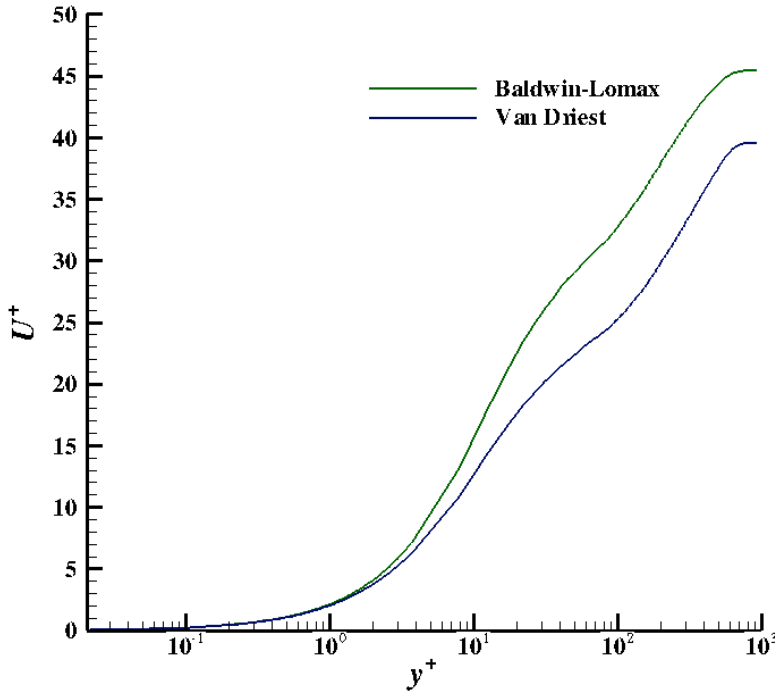


Figure 20:  $U^+$  profile using the Van Driest transformation at  $x=1m$ .

All results have converged to a residual of  $1e^{-9}$ . A better convergence is obtained by using a high Pressure switch factor i.e. 10000. Earlier results didn't converge beyond a residual of  $1e^{-6}$ . A Pressure switch factor = 0.3 was used earlier. Also, the value of  $d_0$  that is denoted by DISS\_BL\_DIST in the input file is set to  $1e^{-2}$  for the laminar case and  $3e^{-1}$  for the turbulent case. Values of  $d_0$  less than this give incorrect flowfield values. This parameter has to be chosen carefully to get correct results.

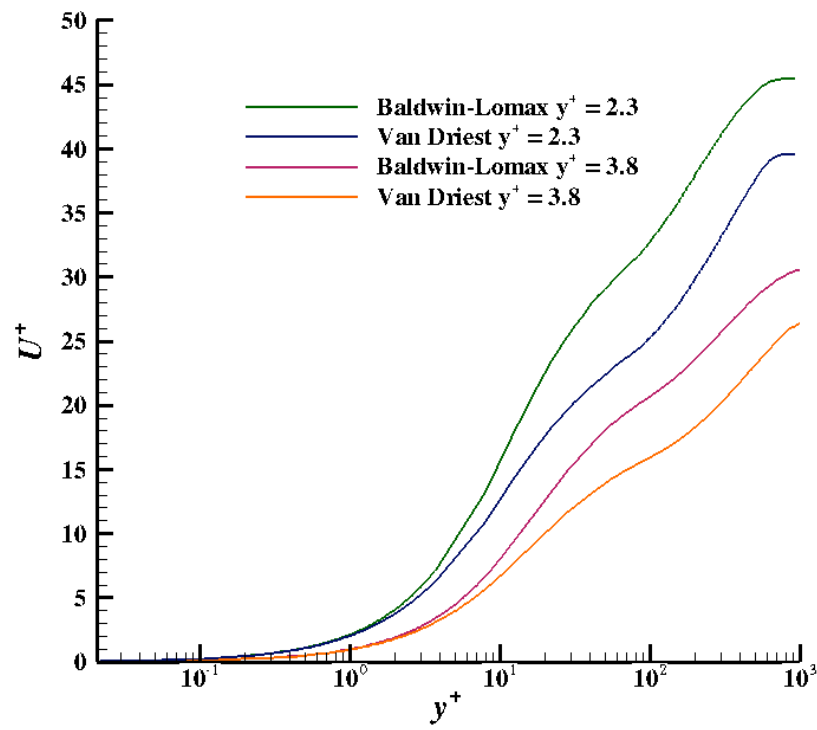


Figure 21:  $U^+$  profile for different values of  $y^+$  at  $x=1m$ .

## 4 Conclusions

Results from the implementation of Baldwin Lomax turbulence model to LeMANS for predicting the turbulent heat transfer and shear stress for hypersonic flow have been presented. The model provides quite good agreement with the measured heat flux and shear stress in the turbulent region. The original and modified Baldwin Lomax model was used in LeMANS for the study. Grid converged solutions were used for comparison with the experimental data and results from other simulations. The modified Baldwin Lomax model that used the local values had better agreement. It was shown that the results were similar for hot wall condition when wall and local values were used but there was a significant difference in the results when cold wall condition was used. It was also shown that the different value of  $A^+$  used in the determination of length scale does not affect the results.

## References

- [1] B. S. Baldwin and H. Lomax. Thin layer approximation and algebraic model I, for separated turbulent flows. Technical report, NASA Ames Research Center, Moffett Field, Cu., 1978.
- [2] Tuncer Cebeci. Calculation of compressible turbulent boundary layers with heat and mass transfer. Number AIAA Paper 70-741. AIAA 3rd Fluid and Plasma Dynamics Conference, June 29 - July 1 1970.
- [3] Tuncer Cebeci. *Analysis of Turbulent Flows (2nd Revised and Expanded Edition)*. Number 978-0-08-044350-8. Elsevier, 2004.
- [4] Arthur D. Dilley. Evaluation of cfd turbulent heating prediction techniques and comparison evaluation of cfd turbulent heating prediction techniques and comparison with hypersonic experimental data. Technical report, NASA/CR-2001-210837, March 2001.
- [5] E. R. Van Driest. On turbulent flow near a wall. *J. Aeronaut. Sci.*, 23, 1956.
- [6] R. N. Gupta, K. P. Lee, E. V. Zoby, J. N. Moss, and R. A. Thompson. Hypersonic viscous shock-layer solutions over long slender bodies. part 1 - high reynolds number flows. *Journal of Spacecraft and Rockets*, 27(2):175–184, March-April 1990.
- [7] M S Holden. An experimental investigation of turbulent boundary layers at high mach number and reynolds numbers. volume Calspan Report No. AB-5072-A-1, NASA CR-112147.
- [8] S. B. Pope. *Turbulent Flows*. Cambridge University Press, 2000.
- [9] Christopher L. Rumsey. Compressibility considerations for k-omega turbulence models in hypersonic boundary-layer applications. *Journal of Spacecraft and Rockets*, Vol. 47(1), January-February 2010.
- [10] Leonardo C. Scalabrin. *Numerical Simulation of Weakly Ionized Hypersonic Flow Over Reentry Capsules*. PhD thesis, University of Michigan, 2007.
- [11] Frank M. White. *Viscous Fluid Flow*. McGraw-Hill, third edition, 2006.